



1 **Holocene dynamics in the Bering Strait inflow to the Arctic and the Beaufort Gyre**  
2 **circulation based on sedimentary records from the Chukchi Sea**

3

4 Masanobu Yamamoto<sup>1-3\*</sup>, Seung-Il Nam<sup>4</sup>, Leonid Polyak<sup>5</sup>, Daisuke Kobayashi<sup>3</sup>, Kenta  
5 Suzuki<sup>3</sup>, Tomohisa Irino<sup>1,3</sup>, Koji Shimada<sup>6</sup>

6

7 <sup>1</sup>*Faculty of Environmental Earth Science, Hokkaido University, Kita-10, Nishi-5,*  
8 *Kita-ku, Sapporo 060-0810 Japan*

9 <sup>2</sup>*Global Institution for Collaborative Research and Education, Hokkaido University,*  
10 *Kita-10, Nishi-5, Kita-ku, Sapporo 060-0810 Japan*

11 <sup>3</sup>*Graduate School of Environmental Science, Hokkaido University, Kita-10, Nishi-5,*  
12 *Kita-ku, Sapporo 060-0810 Japan*

13 <sup>4</sup>*Korea Polar Research Institute, 26 Songdomirae-ro, Yeonsu-gu, Incheon 21990,*  
14 *Republic of Korea*

15 <sup>5</sup>*Byrd Polar and Climate Research Center, The Ohio State University, Columbus, OH*  
16 *43210USA*

17 <sup>6</sup>*Tokyo University of Marine Science and Technology, 4-5-7, Konan, Minato-ku, Tokyo*  
18 *108-8477, Japan.*

19 *\*Corresponding author. Tel: +81-11-706-2379, Fax: +81-11-706-4867, E-mail*  
20 *address: myama@ees.hokudai.ac.jp (M. Yamamoto)*

21

22 **ABSTRACT**

23 The Beaufort Gyre (BG) and the Bering Strait inflow (BSI) are important elements of  
24 the Arctic Ocean circulation system and major controls on the distribution of Arctic sea



25 ice. We report records of the quartz/feldspar and chlorite/illite ratios in three sediment  
26 cores from the northern Chukchi Sea providing insights into the long-term dynamics of  
27 the BG circulation and the BSI during the Holocene. The quartz/feldspar ratio, a proxy  
28 of the BG strength, gradually decreased during the Holocene, suggesting a long-term  
29 decline in the BG strength, consistent with orbitally-controlled decrease in summer  
30 insolation. We suppose that the BG rotation weakened as a result of increasing stability  
31 of sea-ice cover at the margins of the Canada Basin, driven by decreasing insolation.  
32 Millennial to multi-centennial variability in the quartz/feldspar ratio (the BG  
33 circulation) is consistent with fluctuations in solar irradiance, suggesting that solar  
34 activity affected the BG strength on these timescales. The BSI approximated by the  
35 chlorite/illite record shows intensified flow from the Bering Sea to the Arctic during the  
36 middle Holocene, which is attributed primarily to the effect of an overall weaker  
37 Aleutian Low. The middle Holocene intensification of the BSI was associated with  
38 decrease in sea ice concentrations and increase in marine production, as indicated by  
39 biomarker concentrations, suggesting an influence of the BSI on sea ice distribution and  
40 biological production in the Chukchi Sea.

41

## 42 **1. Introduction**

43 The Arctic currently faces rapid climate change caused by global warming (e.g.,  
44 Screen and Simmonds, 2010; Harada, 2016). Changes in the current system of the  
45 Arctic Ocean regulate the state of Arctic sea ice and are involved in global processes via  
46 ice albedo feedback and the delivery of freshwater to the North Atlantic Ocean (Miller  
47 et al., 2010; Screen and Simmonds, 2010). The most significant consequence of this  
48 climate change during recent decades is the retreat of summer sea ice in the Pacific



49 sector of the Arctic (e.g., Shimada et al., 2006; Harada et al., 2016, and references  
50 therein). Inflow of warm Pacific water through the Bering Strait (hereafter Bering Strait  
51 Inflow [BSI]) is suggested to have caused catastrophic changes in sea ice stability in the  
52 western Arctic Ocean (Shimada et al., 2006). Comprehending these changes requires  
53 investigation of a longer-term history of circulation in the western Arctic and its  
54 relationship to atmospheric forcings. Within this context, the Chukchi Sea is a key  
55 region to understand the western Arctic current system as it is located at the crossroads  
56 of the BSI and the Beaufort Gyre (BG) circulation in the western Arctic Ocean (Fig. 1)  
57 (e.g., Winsor and Chapman, 2004; Weingartner et al., 2005).

58 In this paper we apply mineralogical proxies of the BG and BSI to sediment cores  
59 with a century-scale resolution from the northern margin of the Chukchi shelf. The  
60 generated record provides new understanding of changes in the BG circulation and BSI  
61 strength during most of the Holocene (last ~9 ka). We discuss the possible causes and  
62 forcings of the BG and BSI variability, as well as its relationship to sea-ice history and  
63 biological production in the western Arctic.

64

## 65 **2. Background information**

### 66 **2.1. Oceanographic settings**

67 The wind-driven surface current system of the Arctic Ocean consists of the BG and  
68 the Transpolar Drift (TPD) (Proshutinsky and Johnson, 1997; Rigor et al., 2002). This  
69 circulation is controlled by the atmospheric system known as the Arctic Oscillation  
70 (AO) (Rigor et al., 2002). When the AO is in the positive phase, the BG shrinks back  
71 into the Beaufort Sea, the TPD expands to the western Arctic Ocean, and the sea-ice  
72 transport from the eastern Arctic to the Atlantic Ocean is intensified. When the AO is in



73 negative phase, the BG expands, the TPD is limited to the eastern Arctic, and sea ice is  
74 exported efficiently from the Canada Basin to the eastern Arctic. Thus, sea-ice  
75 distribution is closely related to the current system.

76 A dramatic strengthening of the BG circulation occurred during the last two decades  
77 (Shimada et al., 2006; Giles et al., 2012). This change was attributed to a recent  
78 reduction in sea-ice cover along the margin of the Canada Basin, which caused a more  
79 efficient transfer of the wind momentum to the ice and underlying waters in the BG  
80 (Shimada et al., 2006). The delayed development of sea ice in winter enhanced the  
81 western branch of the Pacific Summer Water across the Chukchi Sea. This anomalous  
82 heat flux into the western part of the Canada Basin retarded sea-ice formation during  
83 winter, thus, further accelerating overall sea-ice reduction.

84 The BSI, an important carrier of heat and freshwater to the Arctic, transports the  
85 Pacific water to and across the Chukchi Sea, interacts with the BG circulation at the  
86 Chukchi shelf margin (e.g., Shimada et al., 2006). After passing the Bering Strait the  
87 BSI flows in three major branches. One branch, the Alaskan Coastal Current (ACC),  
88 runs northeastward along the Alaskan coast as a buoyancy-driven boundary current  
89 (Red arrow in Fig. 1; Shimada et al., 2001; Pickart, 2004; Weingartner et al., 2005). The  
90 second, central branch follows a seafloor depression between Herald and Hanna Shoals,  
91 then turns eastward and merges with the ACC (Yellow arrow in Fig. 1; Winsor and  
92 Chapman, 2004; Weingartner et al., 2005). The third branch flows northwestward,  
93 especially when easterly winds prevent the ACC (Winsor and Chapman, 2004). This  
94 branch may then turn eastward along the shelf break (Blue arrow in Fig. 1; Pickart et al.,  
95 2010).



96 The BSI is driven by a northward dip in sea level between the North Pacific and the  
97 Arctic Ocean (Shtokman, 1957; Coachman and Aagaard, 1966). There has been a  
98 long-standing debate, whether this dipping is primarily controlled by steric difference  
99 (Stigebrandt, 1984) or from wind-driven circulations (Gudkovitch, 1962). Stigebrandt  
100 (1984) assumed that the salinity difference between the Pacific and Atlantic Oceans  
101 causes the steric height difference between the Bering Sea and the Arctic Ocean.  
102 Aagaard et al. (2006) argued that the local salinity in the northern Bering Sea controlled  
103 the BSI, although wind can considerably modify the BSI on a seasonal timescale. De  
104 Boer and Nof (2004) proposed a model that the mean sea level difference along the  
105 strait is set up by the global winds, particularly the strong Subantarctic Westerlies.

106 Recently, a conceptual model of the BSI controls has been developed based on a  
107 decade of oceanographic observations (Danielson et al., 2014). According to this model,  
108 storms centered over the Bering Sea excite continental shelf waves on the eastern  
109 Bering shelf that intensify the BSI on synoptic time scales, but the integrated effect of  
110 these storms tends to decrease the BSI on annual to decadal time scales. At the same  
111 time, an eastward shift and overall strengthening of the Aleutian Low pressure center  
112 during the period between 2000–2005 and 2005–2011 increased the sea level pressure  
113 in the Aleutian Basin south of the Bering Strait by 5 hPa, in contrast to overall  
114 decreased pressure of the Aleutian Low system, thus decreasing the water column  
115 density through isopycnal uplift by weaker Ekman suction. This change thereby raised  
116 the dynamic sea surface height by 4.2 m along the Bering Strait pressure gradient,  
117 resulting in the BSI increase by 4.5 cm/s, or 0.2 Sv (calculated based on the  
118 cross-section area of  $4.25 \times 10^6 \text{ m}^2$ ). This increase constitutes about one quarter of the  
119 average long-term BSI volume of  $\sim 0.8 \text{ Sv}$  (Roach et al., 1995). Such a large



120 contribution clearly identifies changes in the Aleutian Low strength and position as a  
121 key factor regulating the BSI on inter-annual time scales.

122 The BSI also transports nutrient from the Pacific to the Arctic. A rough estimation  
123 suggests that the BSI waters significantly contribute to marine production in the Arctic  
124 (Yamamoto-Kawai et al., 2006). High marine production in the Chukchi Sea of up to  
125  $400 \text{ gC m}^{-2} \text{ y}^{-1}$  in part is thought to reflect the high nutrient fluxes by the BSI (Walsh  
126 and Dieterle, 1994; Sakshaug, 2004). A recent enhancement of biological productivity  
127 and the biological pump in the Beaufort and Chukchi Seas has been associated with the  
128 retreat of sea ice (summarized by Harada et al., 2016). This phenomenon is attributed to  
129 an increase of irradiance in the water column (Frey et al., 2011; Lee and Whitledge,  
130 2005), wind-induced mixing that replenishes sea surface nutrients (Carmack et al.,  
131 2006), and their combination (Nishino et al., 2009). However, the nutrient flux into the  
132 Arctic Ocean was not evaluated in this context. The investigation of BSI intensity and  
133 marine production during the Holocene will be useful to understand on-going changes  
134 in marine production in the Arctic Ocean.

135

## 136 ***2.2. Mineral distribution in the Chukchi Sea sediments***

137 Spatial variation in mineral composition of surficial sediments along the western  
138 Arctic margin has been investigated in a number of studies using different  
139 methodological approaches but showing an overall consistent picture (e.g., Naidu et al.,  
140 1982; Naidu and Mowatt, 1983; Wahsner et al., 1999; Kalinenko, 2001; Viscosi-Shirley  
141 et al., 2003; Darby et al., 2011; Kobayashi et al., 2016). A recent study of mineral  
142 distribution in sediments from the Chukchi Sea and adjacent areas of the Arctic Ocean  
143 and the Bering Sea suggests that the quartz/feldspar (Q/F) ratio is higher on the North



144 American than on the Siberian side of the western Arctic (Fig. 2; Kobayashi et al.,  
145 2016). These results are consistent with earlier studies including mineral determinations  
146 of shelf sediments and adjacent coasts (Vogt, 1997; Stein, 2008; Darby et al., 2011). In  
147 particular, data of Darby et al. (2011), although quantified by a different method, also  
148 show a trend of decreasing Q/F ratio from North American margin to the Chukchi Sea  
149 and further to the East Siberian Sea. This zonal gradient of the Q/F ratio suggests that  
150 quartz-rich but feldspar-poor sediments are derived from the North American margin by  
151 the BG circulation, whereas feldspar-rich sediments are delivered to the Chukchi Sea  
152 from the Siberian margin by currents along the East Siberian slope (Kobayashi et al.,  
153 2016). Thus, this ratio can be used as a provenance index for the BG circulation  
154 reflecting changes in its intensity in sediment-core records (Kobayashi et al., 2016).

155 Kaolinite is generally minor clay in the western Arctic but relatively abundant in the  
156 Northwind Ridge and Mackenzie Delta areas where the BG circulation exerts an  
157 influence (Naidu and Mowatt, 1983; Kobayashi et al., 2016). Kaolinite in the  
158 Northwind Ridge originated from ancient rocks exposed on the North Slope and was  
159 delivered by water or sea ice via the Beaufort Gyre circulation (Kobayashi et al., 2016).

160 Kobayashi et al. (2016) also indicate that both the (chlorite + kaolinite)/illite and  
161 chlorite/illite ratios (CK/I and C/I ratios, respectively) are higher in the Bering Sea and  
162 decrease northward throughout the Chukchi Sea, reflecting the diminishing strength of  
163 the BSI (Fig. 2). These results are consistent with earlier studies showing that illite is a  
164 common clay mineral in Arctic sediments (Kalinenko, 2001; Darby et al., 2011),  
165 whereas, chlorite is more abundant in the Bering Sea and the Chukchi shelf areas  
166 influenced by the BSI (Naidu and Mowatt, 1983; Kalinenko, 2001; Nwaodua et al.,  
167 2014; Kobayashi et al., 2016). Chlorite occurs abundantly near the Bering Sea coasts of



168 Alaska, Canada, and the Aleutian Islands (Griffin and Goldberg, 1963). The  
169 chlorite/illite ratio is higher in the bed load of rivers and deltaic sediments from  
170 southwestern Alaska than from northern Alaska and East Siberia, reflecting differences  
171 in the geology of the drainage basins (Naidu and Mowatt, 1983). Because chlorite  
172 grains are more mobile than illite grains under conditions of intense hydrodynamic  
173 activity, chlorite grains are transported a long distance from the northern Bering Sea to  
174 the Chukchi Sea via the Bering Strait (Kalinenko, 2001). In the surface sediments of the  
175 Chukchi Sea, the CK/I ratio shows a good correlation with the C/I ratio, indicating that  
176 both ratios can be used as a provenance index for the BSI (Kobayashi et al., 2016).

177 Ortiz et al. (2009) constructed the first chlorite-based Holocene record of the BSI by  
178 quantifying the total chlorite plus muscovite abundance based on diffuse spectral  
179 reflectance of sediments from a northeastern Chukchi Sea core. The record shows a  
180 prominent intensification of the BSI in the middle Holocene. However, a record from  
181 just one site is clearly insufficient to characterize sedimentation and circulation history  
182 in such a complex area. More records of mineral proxy distribution covering various  
183 oceanographic and depositional environments are needed to further our understanding  
184 of the evolution of the BSI.

185 The Holocene dynamics of the BG circulation is also poorly understood. A study of  
186 sediment core from the northeastern Chukchi slope identified centennial- to  
187 millennial-scale variability in the occurrence of Siberian iron oxide grains presumably  
188 delivered via the BG (Darby et al., 2012). However, transport of these grains depends  
189 not only on the BG, but also on circulation and ice conditions in the Eurasian basin,  
190 which complicates the interpretation and necessitates further proxy studies of the BG  
191 history.





192

### 193 3. Samples and methods

194 This study uses three sediment cores from the northern and northeastern margins of  
195 the Chukchi Sea: ARA02B 01A-GC (gravity core; 563 cm long; 73°37.89'N,  
196 166°30.98'W), HLY0501-05JPC/TC (jumbo piston core/trigger; 1648 cm long,  
197 72°41.68'N, 157°31.20'W) and HLY0501-06JPC (1554 cm long; 72°30.71'N,  
198 157°02.08'W) collected from 111 m, 462 m and 673 water depth, respectively (Fig. 1).

199 The sediments in 01A-GC and in the Holocene part of 05JPC/TC (0–1300 cm) and  
200 06JPC (0–935 cm) consist predominantly of homogeneous clayey silt (fine-grained  
201 unit). This unit of cores 05JPC and 06JPC is underlain by a more complex  
202 lithostratigraphy with laminations and coarse ice rafted debris indicative of  
203 glaciomarine environments affected by glacial/deglacial processes (“glaciomarine unit”;  
204 McKay et al., 2008; Lisé-Pronovost et al., 2009; Polyak et al., 2009).

205 Age was constrained by seven accelerator mass spectrometry (AMS) <sup>14</sup>C ages of  
206 mollusc shells from core 01A-GC (Stein et al., 2017). The core-top of 01A-GC was  
207 assumed to be sediment surface because labile organic compounds such as IP<sub>25</sub> and  
208 sterols show a downcore decreasing trend in their concentrations in the top 10 cm (Stein  
209 et al., 2017), which is commonly seen in ocean surface sediments, suggesting that the  
210 lost of surface sediments was minimal during coring. <sup>14</sup>C ages were converted to  
211 calendar ages using the CALIB7.0 program and marine13 dataset (Reimer et al., 2013).  
212 Local reservoir correction ( $\Delta R$ ) was assumed 500 years for 01A-GC (McNeely et al.,  
213 2006; Darby et al., 2012).

214 In core 05JPC/TC, age was constrained by six AMS <sup>14</sup>C ages of mollusc shells from  
215 core 05JPC (Barletta et al., 2008; Darby et al., 2009). Local reservoir correction ( $\Delta R$ )



216 was assumed 0 years for 05JPC (McNeely et al., 2006; Darby et al., 2012). Concurrent  
217 age constraints for 05JPC were provided by  $^{210}\text{Pb}$  determinations in the upper part  
218 (05TC) and paleomagnetic analysis (Barletta et al., 2008; McKay et al., 2008; Darby et  
219 al., 2012). The age model of core 05JPC/TC was constructed by linear interpolation  
220 between the  $^{14}\text{C}$  datings (2.4–7.7 ka) as well as the assumed modern age of the 05TC  
221 top, with the assumption that the offset of JPC to TC is 75 cm (Polyak et al., 2016).  
222 Ages below the dated range were extrapolated to the bottom of homogenous  
223 fine-grained unit at 1300 cm (9.4 ka).

224 In core 06JPC, age was tentatively constrained by ten paleointensity datums based on  
225 the  $^{14}\text{C}$  ages of nearby cores and a  $^{14}\text{C}$  age of benthic foraminifera (8.16 ka at 918 cm)  
226 (Lisé-Pronovost et al., 2009), with the assumption that the offset of JPC to TC is 147  
227 cm (Ortiz et al., 2009). The age model of core 06JPC was constructed by linear  
228 interpolation between the paleointensity datums (2.0–7.9 ka).

229 In total 110 samples were collected for mineralogical analysis from core 01A-GC at  
230 intervals averaging 5 cm (equivalent to approximately 80–90 years) down to a depth of  
231 545 cm (ca. 9.3 ka). In core 05JPC/TC, 44 samples were collected from fine-grained  
232 unit at intervals averaging 30 cm (equivalent to approximately 210–220 years) down to  
233 a depth of 1286 cm (ca. 9.3 ka), and 7 samples were collected from the underlying  
234 glaciomarine sediments. In core 06JPC, 79 samples were collected from fine-grained  
235 unit at intervals of 10 cm (equivalent to approximately 90 years) down to a depth of 937  
236 cm (ca. 8.0 ka), and 46 samples were collected from the underlying glaciomarine unit.

237 We also analyzed 16 surface sediment samples (0–1 cm) from the eastern Beaufort  
238 Sea near Mackenzie delta and 3 surface sediment samples (0–1 cm) from the western  
239 Beaufort Sea (Fig. 2) to fill the gaps in the dataset of Kobayashi et al. (2016). These



240 were obtained during the RV Araon cruises in 2013 and 2014 (ARA04C and ARA05C,  
241 respectively; supplementary table 1).

242 Mineral composition was analyzed on MX-Labo X-ray diffractometer (XRD)  
243 equipped with a CuK $\alpha$  tube and monochromator. The used tube voltage and current  
244 were 40 kV and 20 mA, respectively. Scanning speed was 4°2 $\theta$ /min and the data  
245 sampling step was 0.02°2 $\theta$ . Each powdered sample was mounted on a glass holder with  
246 a random orientation and X-rayed from 2 to 40°2 $\theta$ . An additional precise scan with a  
247 scanning speed of 0.2°2 $\theta$ /min and sampling step of 0.01°2 $\theta$  from 24 to 27°2 $\theta$  was  
248 conducted to distinguish chlorite from kaolinite by evaluation of the peaks around  
249 25.1°2 $\theta$  (Elvelhøi and Rønningsland, 1978). In this study, the background-corrected  
250 diagnostic peak intensity was used for evaluating the abundance of each mineral. The  
251 relative XRD intensities of quartz at 26.6°2 $\theta$  (d = 3.4 Å), feldspar including both  
252 plagioclase and K-feldspar at 27.7°2 $\theta$  (d = 3.2 Å), illite including mica at 8.8°2 $\theta$  (d =  
253 10.1 Å), chlorite including kaolinite (called “chlorite+kaolinite” hereafter) at 12.4°2 $\theta$  (d  
254 = 7.1 Å), kaolinite at 24.8 °2 $\theta$  (d = 3.59 Å) and chlorite at 25.1°2 $\theta$  (d = 3.54 Å) were  
255 determined using MacDiff software (Petschick, 2000) based on the peak identification  
256 protocols of Biscaye (1965).

257 The mineral ratios used in this study are defined based on XRD peak intensities (PI)  
258 as:

259  $Q/F = \text{quartz/feldspar} = [\text{PI at } 26.6^\circ 2\theta] / [\text{PI at } 27.7^\circ 2\theta]$

260  $CK/I = (\text{chlorite+kaolinite})/\text{illite} = [\text{PI at } 12.4^\circ 2\theta] / [\text{PI at } 8.8^\circ 2\theta]$

261  $C/I = \text{chlorite}/\text{illite} = [\text{PI at } 25.1^\circ 2\theta] / [\text{PI at } 8.8^\circ 2\theta]$

262  $K/I = \text{kaolinite}/\text{illite} = [\text{PI at } 24.8^\circ 2\theta] / [\text{PI at } 8.8^\circ 2\theta]$



263 The standard error of duplicate analyses in all samples averaged 1.1, 0.08 and 0.05  
264 for Q/F, CK/I and C/I ratios, respectively.

265 Clay minerals (less than 2- $\mu\text{m}$  diameter) in core 01A-GC were separated by the  
266 settling method based on the Stokes' law (Müller, 1967). To produce an oriented powder  
267 X-ray diffractometry (XRD) sample, the collected clay suspensions were  
268 vacuum-filtered onto 0.45- $\mu\text{m}$  nitrocellulose filters and dried. Ethylene glycol (50  $\mu\text{l}$ )  
269 was then soaked onto the oriented clay on the filters. Glycolated sample filters were  
270 stored in an oven at 70°C for four hours and then immediately subjected to XRD  
271 analyses. Each sample filter was placed directly on a glass slide and X-rayed with a tube  
272 voltage of 40 kV and current of 20 mA. Scanning speed was 0.5°/min and the  
273 data-sampling step was 0.02° from 2 to 15°. An additional precise scan with a  
274 scanning speed of 0.2°/min and sampling step of 0.01° from 24 to 27° was  
275 conducted to distinguish chlorite from kaolinite by evaluation of the peaks around  
276 25.1° (Elvelhøi and Rønningsland, 1978). The standard errors of duplicate analyses in  
277 all samples averaged 0.05 and 0.06 for CK/I and C/I ratios, respectively.

278 The diffraction intensity of chlorite+kaolinite at 7.1 Å was significantly positively  
279 correlated with that of chlorite at 3.54 Å ( $r = 0.89$ ), but not with that of kaolinite at 3.59  
280 Å ( $r = 0.39$ ) in western Arctic surface sediments (Kobayashi et al., 2016), indicating that  
281 the diffraction intensity of chlorite+kaolinite is governed by the amount of chlorite rather  
282 than that of kaolinite.

283 Spectral analysis of the downcore Q/F and C/I variability was performed using the  
284 maximum entropy method provided in the Analyseries software package (Paillard et al.,  
285 1996).

286



287 **4. Results**

288 **4.1. Surface sediments of the Beaufort Sea**

289 Because the dataset of Kobayashi et al. (2016) has only one sample in the eastern  
290 Beaufort Sea, we added the data of 16 samples from the eastern Beaufort Sea near the  
291 Mackenzie delta and 3 samples from the western Beaufort Sea to fill the gaps in their  
292 dataset. More clearly than Kobayashi et al. (2016), the new combined dataset shows that  
293 the surface sediments in the eastern Beaufort Sea have the higher Q/F and lower CK/I  
294 and C/I ratios than those in the Chukchi Sea (Fig. 2A–C; Supplementary table 1).

295 The Q/F ratio showed a westward decreasing trend from the eastern Beaufort Sea to  
296 the East Siberian Sea and its offshore area (Fig. 2D). This supports a notion that  
297 quartz-rich but feldspar-poor sediments are derived from the North American margin by  
298 the BG circulation, whereas feldspar-rich sediments are delivered to the Chukchi Sea  
299 from the Siberian margin by currents along the East Siberian slope (Vogt, 1997; Stein,  
300 2008; Darby et al., 2011; Kobayashi et al., 2016).

301 The CK/I and C/I ratios showed a northward decreasing trend in the Chukchi Sea and  
302 the Chukchi Borderland (Fig. 2E). This result are consistent with earlier studies  
303 showing that illite is a common clay mineral in Arctic sediments (Kalinenko, 2001;  
304 Darby et al., 2011), whereas, chlorite is more abundant in the Bering Sea and the  
305 Chukchi shelf areas influenced by the BSI (Naidu and Mowatt, 1983; Kalinenko, 2001;  
306 Nwaodua et al., 2014; Kobayashi et al., 2016).

307 These trends support the conclusion of Kobayashi et al. (2016) mentioning that the  
308 Q/F ratio can be used as a provenance index for the BG circulation reflecting a  
309 westward decrease in its intensity, and the CK/I and C/I ratios can be used as a  
310 provenance index for the BSI reflecting a northward decrease in its intensity. The



311 provenance and transportation of these detrital minerals are discussed in detail in Naidu  
312 and Mowatt (1983), Kalinenko (2001), Nwaodua et al. (2014) and Kobayashi et al.  
313 (2016).

314

#### 315 **4.2. Cores 01A-GC, 05JPC/TC and 06JPC**

316 Quartz, feldspar including plagioclase and K-feldspar, illite, chlorite, kaolinite and  
317 dolomite were detected in the study samples. Plagioclase comprises a variety of  
318 anorthite to albite. Microscopic observations of smear slides for the study samples  
319 revealed that quartz and feldspar are the two major minerals in the composition of  
320 detrital grains.

321 The variation patterns of the Q/F, C/I, CK/I and K/I ratios are different between  
322 fine-grained and glaciomarine units in cores 05JPC/TC and 06JPC (Fig. 3;  
323 Supplementary tables 2–4). The ratios of fine-grained unit are relatively stable  
324 compared with those in glaciomarine units. The higher Q/F ratio in glaciomarine units is  
325 consistent with the finding of previous studies that quartz grains are abundant in the  
326 western Arctic sediments delivered from the Laurentide ice sheet during glacial and  
327 deglacial periods (Bischof et al., 1996; Bischof and Darby, 1997; Phillips and Grantz,  
328 2001; Kobayashi et al., 2016). Some peaks correspond to dolomite-rich layers (“D” in  
329 Fig. 3). Variation in the K/I ratio was associated with that in the Q/F ratio (Fig. 3),  
330 which is in harmony with an idea that kaolinite was delivered via the Beaufort Gyre  
331 circulation (Kobayashi et al., 2016). The C/I and CK/I ratios are lower in glaciomarine  
332 unit than in fine-grained unit in 06JPC (Fig. 3C), which is consistent with the closure of  
333 Bering Strait in the last glacial (Elias et al., 1992), but this difference is not significant  
334 in 05JPC (Fig. 3B).



335 The Q/F ratio in cores 01A-GC, 05JPC/TC and 06JPC shows a gradual long-term  
336 decrease throughout the Holocene (Fig. 4A). In cores 01A-GC and 06JPC studied in  
337 more detail, the Q/F ratio also indicates millennial- to century-scale variability (Fig. 4A).  
338 Variations of the 5-point running average highlight millennial-scale patterns (Fig. 4A).  
339 The variations are generally asynchronous between both cores on this timescale, which  
340 strongly depends on their age-depth models.

341 In core 01A-GC, the CK/I and C/I ratios show a general increase after ca. 9.5 ka with  
342 the highest values occurring between 6 and 4 ka, and high ratios around 2.5 ka and 1 ka  
343 (Fig. 4B). In core 06JPC, the ratios show a general increase after 9.2 ka with higher  
344 values occurring between 6 and 3 ka (Fig. 4B). In core 05JPC/TC, slightly higher ratios  
345 occur between 6 and 3 ka after a gradual increase from 9.3 ka (Fig. 4B).

346

## 347 **5. Discussion**

### 348 ***5.1. Holocene trend in the Beaufort Gyre circulation***

349 The zonal gradient of the Q/F ratio in western Arctic sediments shown in Fig. 2  
350 suggests that quartz-rich but feldspar-poor sediments are derived from the North  
351 American margin by the BG circulation, whereas feldspar-rich sediments are delivered  
352 to the Chukchi Sea from the Siberian margin by currents along the East Siberian slope,  
353 and the ratio can be used as an index for the BG circulation reflecting changes in its  
354 intensity in sediment-core records (Kobayashi et al., 2016). A consistent upward  
355 decrease in the Q/F ratio in three different cores under study (Fig. 4A) suggests that the  
356 BG weakened during the Holocene. This pattern is consistent with an orbitally-forced  
357 decrease in summer insolation at northern high latitudes from the early Holocene to  
358 present. High summer insolation likely melted sea ice in the Canada Basin, in particular



359 in the coastal areas (Fig. 5). The evidence of lower ice concentrations at the Canada  
360 Basin margins in the early Holocene was shown in the fossil records of bowhead whale  
361 bones from the Beaufort Sea coast (Dyke and Savelle, 2001) and driftwood from  
362 northern Greenland (Funder et al., 2011). This condition could decrease the stability of  
363 the ice cover at the margins of the Canada Basin, which accelerated the rotation of the  
364 BG circulation (Fig. 5), by comparison with observations from recent decades (Shimada  
365 et al., 2006). A decrease in summer insolation during the Holocene should have  
366 increased the stability of sea-ice cover along the coasts, resulting in the weakening of  
367 the BG.

368 Recent observations show that the BG circulation is linked to the AO (Proshutinsky  
369 and Johnson, 1997; Rigor et al., 2002). In the negative phase of the AO, the Beaufort  
370 High strengthens and intensifies the BG. If the gradual weakening of the BG during the  
371 Holocene were attributed to atmospheric circulation only, a concurrent shift in the mean  
372 state of the AO from the negative to positive phase would be expected. This view,  
373 however, contradicts the existing reconstructions of the AO history showing multiple  
374 shifts between the positive and negative phase during the Holocene (e.g., Rimbu et al.,  
375 2003; Olsen et al., 2012). We, thus, infer that the decreasing Holocene trend of the BG  
376 circulation is attributed not to changes in the AO pattern, but rather to the increasing  
377 stability of the sea-ice cover in the Canada Basin.

378 Based on a Holocene sediment record off northeastern Chukchi margin, Darby et al.  
379 (2012) suggested strong positive AO-like conditions between 3 and 1.2 ka based on  
380 abundant ice-rafted iron oxide grains from the West Siberian shelf. In contrast, a mostly  
381 negative AO in the late Holocene can be inferred from mineralogical proxy data  
382 indicating a general decline of the BSI after 4 ka (Ortiz et al., 2009), which could be





383 attributed to a stronger Aleutian Low (Danielson et al., 2014) that typically corresponds  
384 to the negative AO (Overland et al., 1999). Olsen et al. (2012) also concluded that the  
385 AO tended to be mostly negative from 4.2 to 2.0 ka based on a redox proxy record from  
386 a Greenland lake. In order to comprehend these patterns, we need to consider not only  
387 the atmospheric circulation, but also sea-ice conditions. Based on the Q/F record in this  
388 study, summer Arctic sea-ice cover shrank in the early to middle Holocene, so that fast  
389 ice containing West Siberian grains could less effectively reach the Canada Basin  
390 because sea ice would have melted on the way to the BG (Fig. 5). Later in the Holocene  
391 the ice cover expanded, and West Siberian fast ice could survive and be incorporated  
392 into the BG (Fig. 5). We infer, therefore, that sediment transportation in the BG is  
393 principally governed by the distribution of summer sea ice and the resultant stability of  
394 the ice cover in the Canada Basin.

395

### 396 ***5.2. Millennial variability in the BG circulation***

397 In addition to the decreasing long-term trend, the Q/F ratio in 01A-GC and 06JPC  
398 clearly displays millennial- to century-scale variability (Fig. 4A). Variation in the Q/F  
399 ratio of both 01A-GC and 06JPC indicates a significant periodicity of ~2100 and ~1000  
400 years with weak periodicities of ~500 and ~360 years, consistent with prominent  
401 periodicities in the variation of total solar irradiance (Fig. 6) (Steinilber et al., 2009). A  
402 comparison with the record of total solar irradiance (Steinilber et al., 2009) shows a  
403 general correspondence, where stronger BG circulation (higher Q/F ratio) corresponds  
404 to higher solar irradiance (Fig. 7). A ~200-year phase lag between the solar irradiance  
405 and the Q/F ratio in 01A-GC and 06JPC may be attributed to the underestimation of  
406 local carbon reservoir effect. This pattern suggests that millennial-scale variability in



407 the BG was principally forced by changes in solar irradiance. Because these changes are  
408 energetically much smaller than changes in the summer insolation caused by orbital  
409 forcing, we suppose that solar activity did not directly affect the stability of ice cover in  
410 the Canada Basin. Alternatively, we suggest that the solar activity signal was amplified  
411 by positive feedback mechanisms, possibly through changes in the stability of sea-ice  
412 cover and/or the atmospheric circulation in the northern high latitudes.

413 In addition to cycles consistent with the solar forcing, Darby et al. (2012) reported a  
414 1,550 year cycle in the Siberian grain variation in the Chukchi Sea record. This cycle  
415 was, however, not detected in our data indicative of the BG variation (Fig. 6). This  
416 difference suggests that the occurrence of Siberian grains in the Chukchi Sea sediments  
417 primarily reflects the formation and transportation of fast ice in the eastern Arctic Ocean  
418 rather than changes in the BG circulation.

419

### 420 ***5.3. Holocene changes in the Bering Strait Inflow***

421 Northward decreasing trends in the CK/I and C/I ratios in surface sediments in the  
422 Chukchi Sea suggests that chlorite-rich sediments are derived from the northern Bering  
423 Sea via Bering Strait, and the ratios can be used as an index for the BSI reflecting  
424 changes in its intensity in sediment-core records (Kobayashi et al., 2016). Although the  
425 variations of the CK/I and C/I ratios are not identical among three study cores (Fig. 4B),  
426 there is a common long-term trend showing a gradual increase from 9 to 4.5 ka and a  
427 decrease afterwards (Fig. 4B). Large fluctuation is significant in 01A-GC from 6 to 4 ka,  
428 and this fluctuation is also seen in 6JPC to some extent (Fig. 4B).

429 The higher CK/I and C/I ratios in core 01A-GC in the middle Holocene correspond to  
430 higher linear sedimentation rates estimated by interpolation between  $^{14}\text{C}$  dating points,



431 but this correspondence is not seen in cores 05JPC/TC and 06JPC (Fig. 4C). We assume  
432 that these higher sedimentation rates at 01A-GC indicate intensified BSI, because fine  
433 sediment in the study area is mostly transported by currents from the Bering Sea and  
434 shallow southern Chukchi shelf (Kalinenko, 2001; Darby et al., 2009; Kobayashi et al.,  
435 2016). The difference of chlorite and sedimentation rate records between 01A-GC and  
436 05JPC/06JPC may be related to either 1) variable sediment focusing at different water  
437 depths, or 2) redistribution of the BSI water between different branches after passing the  
438 Bering Strait. 1) A sediment-trap study demonstrated that shelf-break eddies in winter  
439 are important to carry fine-grained lithogenic material from the Chukchi Shelf to the  
440 slope areas (Watanabe et al., 2014). This redeposition process may have weakened the  
441 BSI signal in slope sediments of 05JPC/06JPC compared with outer shelf sediments of  
442 01A-GC. 2) Both the Alaskan Coastal Current (ACC) and the central current can  
443 transport sediment particles to the 05JPC/TC and 06JPC area (red and yellow arrows,  
444 respectively, in Fig. 1; Winsor and Chapman, 2004; Weingartner et al., 2005). In  
445 comparison, the western branch is more likely to carry sediment particles to the site of  
446 01A-GC (blue arrow in Fig. 1). Redistribution of the BSI water may have caused  
447 different response of BSI signals. Although it is not clear which process made the  
448 difference of BSI signals between 01A-GC and 05JPC/06JPC cores, it is highly possible  
449 that the sedimentation rate and mineral composition of 01A-GC are more sensitive to  
450 changes in BSI intensity than those of two other sites.

451 Diffuse spectral reflectance in core HLY0501-06JPC indicated that chlorite +  
452 muscovite content is especially high in the middle Holocene between ca. 4 and 6 ka  
453 (Supplementary Fig. S1; Ortiz et al., 2009). However, this pattern was not confirmed by  
454 our XRD analysis, where XRD intensities of chlorite and muscovite (detected as illite in



455 this study) as well as the  $C/I$  and  $CK/I$  ratios did not show an identifiable enrichment  
456 between 4 and 6 ka (Supplementary Fig. S1). We need more research to understand the  
457 discrepancy of the results.

458

#### 459 ***5.4. Millennial variability in the BSI***

460 Variation in the  $C/I$  ratio of 01A-GC indicates a significant periodicity of 1900, 1000,  
461 510, 400 and 320 years (Fig. 6A). The 1900, 1000 and 510 years are consistent with  
462 prominent periodicities in the variation of total solar irradiance (Fig. 6C) (Steinhilber et  
463 al., 2009). On the other hands, variation in the  $C/I$  ratio of 06JPC indicates a periodicity  
464 of 2200, 830 and 440 years (Fig. 6B). The periodicity is different from that in 01A-GC  
465 (Fig. 6A). This suggests that there are different agents of BSI signals in cores 01A-GC  
466 and 06JPC. In core 01A-GC, 1000-year filtered variation in the  $C/I$  ratio is nearly  
467 antiphase with those of the  $Q/F$  ratio and total solar irradiance (Steinhilber et al., 2009)  
468 between 0 and 5 ka (Fig. 7). This suggests that millennial-scale variability in the  
469 western branch of the BSI was forced by changes in solar irradiance after 5 ka. Recent  
470 observations demonstrated that the BSI flows northwestward, especially when easterly  
471 winds prevent the ACC (Winsor and Chapman, 2004). Because the easterly winds drive  
472 the BG circulation, this mechanism cannot explain the increase of BSI intensity when  
473 the BG weakened. Alternatively, it is also possible that the solar forcing could  
474 independently regulate the western branch of the BSI via unknown atmospheric-oceanic  
475 dynamics.

476

#### 477 ***5.5. Ocean circulation, sea ice and biological production***



478 The BSI, an important carrier of heat to the Arctic, affects sea ice extent in the  
479 Chukchi Sea (e.g., Shimada et al., 2006). Sea ice concentrations in the Chukchi Sea  
480 during the Holocene were reconstructed by dinoflagellate cyst (de Vernal et al., 2005;  
481 2008; 2013; Farmer et al., 2011) and biomarker IP<sub>25</sub> (Polyak et al., 2016; Stein et al.,  
482 2017).

483 In central northern Chukchi Sea, IP<sub>25</sub> records showed that sea ice concentration  
484 indicated by PIP<sub>25</sub> index in core 01A-GC was lower in 9–7.5 ka and 5.5–4 ka (Fig. 8A;  
485 Stein et al., 2017), suggesting less sea ice conditions in the periods. The low sea ice  
486 concentration during 9–7.5 ka is consistent with the results of previous studies based on  
487 dinoflagellate cyst and IP<sub>25</sub> records showing the sea ice retreat widely in the Arctic  
488 Ocean, which was attributed to higher summer insolation during the early Holocene  
489 (Dyke and Savelle, 2001; Vare et al., 2009; de Vernal et al., 2013; Stein et al., 2017).  
490 On the other hands, the sea ice retreat during 5.5–4 ka cannot be explained by higher  
491 summer insolation. This period corresponds to that of higher C/I and CK/I ratios  
492 indicative of the stronger BSI at 01A-GC (Fig. 8A). This suggests that the strengthened  
493 BSI during this period contributed to sea ice retreat in the central Chukchi Sea.

494 In the northeastern Chukchi Sea, dinoflagellate cyst and biomarker IP<sub>25</sub> records from  
495 several cores in the northeastern Chukchi Sea, including 05JPC, demonstrate that sea  
496 ice concentration in this area was overall higher in the early Holocene than in the  
497 middle and late Holocene (Fig. 8; de Vernal et al., 2005; 2008; 2013; Farmer et al.,  
498 2011; Polyak et al., 2016). This pattern appears to contrast reconstructions from other  
499 Arctic regions that show lower sea-ice concentrations in the early Holocene (de Vernal  
500 et al., 2013). This discrepancy suggests that the intensified BG circulation exported  
501 more ice from the Beaufort Sea to the northeastern Chukchi Sea margin. Furthermore,



502 the heat transport from the North Pacific to the Arctic Ocean by the BSI was likely  
503 weaker in the early Holocene than at later times as indicated by the C/I and CK/I ratios  
504 of cores 06JPC and 01A-GC (Fig. 8). We infer that this combination of stronger BG  
505 circulation and weaker BSI in the early Holocene resulted in increased sea-ice  
506 concentration in the northeastern Chukchi Sea despite high insolation levels (Fig. 5). In  
507 comparison, intense BSI, a crucial agent of heat transport from the North Pacific to the  
508 Arctic Ocean, along with weaker BG in the middle Holocene likely reduced sea ice  
509 cover in the Chukchi Sea. During the late Holocene, characterized by the weakest BG  
510 and moderate BSI, sea-ice concentrations were intermediate and strongly variable (Fig.  
511 8; de Vernal et al., 2008, 2013; Polyak et al., 2016).

512 The nutrient supply by the BSI potentially affects marine production in the Chukchi  
513 Sea. We tested this possibility to compare our BSI record with marine production  
514 records from cores 01A-GC (Park et al., 2016; Stein et al., 2017). Isoprenoid GDGTs  
515 and brassicaterol showed concentration maxima during the periods between 8 and 7.5  
516 ka and 6 and 4.5 ka (Fig. 8A). Isoprenoid GDGTs are produced by marine Archaea  
517 (Nishihara et al., 1987) that use ammonia, urea and organic matter in the water column  
518 (Qin et al., 2014). Brassicasterol is known as a sterol which is abundant in diatoms  
519 (Volkman et al., 1986). Their abundance can, thus, be used as proxies to indicate marine  
520 production in the water column. The periods with abundant isoprenoid GDGTs and  
521 brassicasterol corresponded to the periods of low PIP<sub>25</sub> indicative of less sea ice (Fig.  
522 8A). This correspondence suggests that the biological productivity increased with the  
523 retreat of sea ice in the Chukchi Sea during the middle Holocene. The BSI indices, the  
524 C/I and CK/I ratios, showed a maximum between 6 and 4 ka, which corresponded to the  
525 periods of high marine production, but the corresponding maximum between 8 and 6.5



526 ka is not significant. Also, correspondence between the BSI indices and biomarker  
527 concentrations are not clear after 4 ka. This suggests that marine production was not a  
528 simple response to nutrient supply but was affected by other processes such as the  
529 increase of irradiance in the water column (Frey et al., 2011; Lee and Whitley, 2005)  
530 and wind-induced mixing that replenishes sea surface nutrients (Carmack et al., 2006).

531

### 532 *5.6. Causes of BSI variations*

533 Chukchi Sea sedimentary core records indicate a considerable variability in the BSI  
534 intensity, with a common long-term trend of a gradual increase from 9 to 4.5 ka and a  
535 decrease afterwards (Fig. 4B). Below we discuss the possible controls on this  
536 variability.

537 The timing of the initial postglacial flooding of the ~50-m-deep Bering Strait was  
538 estimated as between ca. 12 and 11 ka (Elias et al., 1992; Keigwin et al., 2006). Gradual  
539 intensification of the BSI inferred from the increase in chlorite content from ca. 9 to 6  
540 ka may have been largely controlled by the widening and deepening of the Bering Strait  
541 with rising sea level, although other factors as discussed below yet need to be tested.  
542 After the sea level rose to nearly present position by ca. 6 ka, its influence on changes in  
543 the BSI volume was negligible.

544 The possible driving forces of the BSI at full interglacial sea level may include  
545 several controls. One is related to the sea surface height difference between the Pacific  
546 and Atlantic Oceans regulated by the atmospheric moisture transport from the Atlantic  
547 to the Pacific Ocean across Central America (Stigebrandt, 1984). Increase in this  
548 moisture transport during warm climatic intervals (Leduc et al., 2007; Richter and Xie,  
549 2010; Singh et al., 2016) may have intensified the BSI. Salinity proxy data for the last



550 90 ka from the Equatorial East Pacific confirm increased precipitation during warm  
551 events, but also show the trans-Central America moisture transport may operate  
552 efficiently only during intervals with a northerly position of the Intertropical  
553 Convergence Zone due to orographic constraints (Leduc et al., 2007). The existing  
554 Holocene salinity records from the North Pacific (e.g., Sarnthein et al., 2004) do not yet  
555 provide sufficient material to test the impact of these changes on the BSI.

556 Interplay of the global wind field and the AMOC has been proposed as another  
557 potential control on the BSI (De Boer and Nof, 2004; Ortiz et al., 2012). Results of an  
558 analytical ocean modeling experiment (Sandal and Nof, 2008) based on the island rule  
559 (Godfrey, 1989) suggest that weaker Subantarctic Westerlies in the middle Holocene  
560 could decrease the near surface, cross-equatorial flow from the Southern Ocean to the  
561 North Atlantic, thus enhancing the BSI and Arctic outflow into the Atlantic. This  
562 hypothesis waits to be tested more thoroughly, including robust proxy records of the  
563 Subantarctic Westerlies over the Southern Ocean.

564 Finally, BSI can be controlled by the regional wind patterns in the Bering Sea  
565 (Danielson et al., 2014), as explained above in Section 2.1. Oceanographic observations  
566 of 2000–2011 clearly show a decadal response of the BSI to a change in the sea level  
567 pressure in the Aleutian Basin affecting the dynamic sea surface height along the Bering  
568 Strait pressure gradient. In order to conclude, if this relationship holds on longer time  
569 scales, longer-term records are needed from areas affected by the BSI and the Bering  
570 Sea pressure system.

571 A number of proxy records from the Bering Sea and adjacent regions, both marine  
572 and terrestrial, have been used to characterize paleoclimatic conditions related to  
573 changes in the Bering Sea pressure system (e.g., Barron et al., 2003; Anderson et al.,





574 2005; Katsuki et al., 2009; Barron and Anderson, 2011; Osterberg et al., 2014). Various  
575 proxies used in these records consistently show that the Aleutian Low was overall  
576 weaker in the middle Holocene than in the late Holocene, opposite to the BSI strength  
577 inferred from our Chukchi Sea data (Fig. 4B). For example, multi-proxy data from the  
578 interior Alaska and adjacent territories (Kaufman et al., 2016, and references therein)  
579 indicate overall drier and warmer conditions in the middle Holocene, consistent with  
580 weaker Aleutian Low and stronger BSI. Diatom records from southern Bering Sea  
581 indicate more abundant sea ice in the middle Holocene, also suggestive of a weaker  
582 Aleutian Low (Katsuki et al., 2009). Alkenone and diatom records from the California  
583 margin show that the sea surface temperature was lower in the middle Holocene,  
584 suggesting stronger northerly winds indicative of weaker Aleutian Low (Barron et al.,  
585 2003). Intensification of the Aleutian Low in the late Holocene, which follows from  
586 these results, would have decreased sea level pressure in the Aleutian Basin, and thus  
587 the strength of the BSI, consistent with overall lower BSI after ca. 4 ka inferred from  
588 the Chukchi Sea sediment-core data (Fig. 4). A considerable climate variability of the  
589 Bering Sea region captured in the upper Holocene records, some of which have very  
590 high temporal resolution, is also closely linked to the pressure system changes  
591 (Anderson et al., 2005; Porter, 2013; Osterberg et al., 2014; Steinman et al., 2014). In  
592 particular, weakening of the Aleutian Low is reflected in Alaskan ice (Porter, 2013;  
593 Osterberg et al., 2014) and lake cores (Anderson et al., 2005; Steinman et al., 2014) at  
594 intervals centered around ca. 2 and 1–0.5 ka BP, which may correspond to BSI  
595 increases in the Chukchi core 01A-GC at ca. 2.5 and 1 ka BP (Fig. 4), considering the  
596 uncertainties of the sparse age constraints in the upper Holocene and/or underestimation  
597 of reservoir ages. Overall, the Aleutian Low control on the BSI on century to millennial



598 time scales is corroborated by ample proxy data in comparison with the other potential  
599 controls, although more evidence is still required for a comprehensive interpretation.

600

## 601 **6. Conclusions**

602 The sedimentary proxy-based reconstruction of the BG weakening during the  
603 Holocene, likely driven by the orbitally-controlled summer insolation decrease,  
604 indicates basin-wide changes in the Arctic current system and suggests that the stability  
605 of sea ice is a key factor regulating the Arctic Ocean circulation on the long-term (e.g.,  
606 millennial) time scales. This conclusion helps to better understand a dramatic change in  
607 the BG circulation during the last decade, probably caused by sea-ice retreat along the  
608 margin of the Canada Basin and a more efficient transfer of the wind momentum to the  
609 ice and underlying waters (Shimada et al., 2006). These results suggest that the rotation  
610 of the BG is likely to be further accelerated by the projected future retreat of summer  
611 Arctic sea ice. Millennial to multi-centennial variability in the quartz/feldspar ratio (the  
612 BG circulation) is consistent with fluctuations in solar irradiance, suggesting that solar  
613 activity affected the BG strength on these timescales.

614 Our results on clay-mineral ratios quantifying inputs of chlorite from the Bering Sea  
615 to sediments at the northern Chukchi margin provide a robust record of the strength of  
616 the BSI during the Holocene. We conclude that BSI variability after the establishment  
617 of the full interglacial sea level was primarily controlled by the Bering Sea pressure  
618 system (strength and position of the Aleutian Low). Details of this mechanism, as well  
619 as contributions from other potential BSI controls, such as climatically-driven  
620 Atlantic-Pacific moisture transfer and the impact of global wind stress, need to be  
621 further investigated.



622

623 **Acknowledgements**

624 We thank all of the captain, crew and scientists of RV *Araon* for their help during the  
625 cruise of sampling. We also thank Yu-Hyeon Park, Anne de Vernal, Seth L. Danielson,  
626 Julie Brigham-Grette and Kaustubh Thirumalai for valuable discussion, So-Young Kim,  
627 Hyo-Sun Ji, Young-Ju Son, Duk-Ki Han and Hyoung-Jun Kim for assistance in coring  
628 and subsampling and Keiko Ohnishi for analytical assistance. The study was supported  
629 by a grant-in-aid for Scientific Research (B) the Japan Society for the Promotion of  
630 Science, No. 25287136 (to M.Y.) and Basic Research Project (PE16062) of Korean  
631 Polar Research Institute and the NRF of Korea Grant funded by the Korean Government  
632 (NRF-2015M1A5A1037243) (to S.I.N.).

633

634 **References**

- 635 Aagaard, K., Weingartner, T.J., Danielson, S. L., Woodgate, R.A., Johnson, G. C., and  
636 Whitlege, T.E.: Some controls on flow and salinity in Bering Strait, *Geophysical*  
637 *Research Letters*, 33, L19602, 2006.
- 638 Anderson, L, Abbott, M.B., Finney, B.P., and Burns, S.J.: Regional atmospheric  
639 circulation change in the North Pacific during the Holocene inferred from lacustrine  
640 carbonate oxygen isotopes, Yukon Territory, Canada, *Quaternary Research*, 64, 21–  
641 35, 2005.
- 642 Barletta, F. et al.: High resolution paleomagnetic secular variation and relative  
643 paleointensity records from the western Canadian Arctic: implication for Holocene  
644 stratigraphy and geomagnetic field behaviour, *Canadian Journal of Earth Sciences*,  
645 45, 1265–1281, 2008.



- 646 Barron, J.A. and Anderson, L.: Enhanced Late Holocene ENSO/PDO expression along  
647 the margins of the eastern North Pacific, *Quaternary International*, 235, 3–12, 2011.
- 648 Barron, J.A., Heusser, L., Herbert, T., and Lyle, M.: High-resolution climatic evolution  
649 of coastal northern California during the past 16,000 years, *Paleoceanography*, 18,  
650 1020, 2003.
- 651 Biscaye, P.: Mineralogy and sedimentation of recent deep-sea clay in the Atlantic  
652 Ocean and adjacent seas and oceans, *Geological Society of America Bulletin*, 76,  
653 803–832, 1965.
- 654 Bischof, J., Clark, D.L., and Vincent, J.S.: Origin of ice rafted debris: Pleistocene  
655 paleoceanography in the western Arctic Ocean, *Paleoceanography*, 11, 743–756,  
656 1996.
- 657 Bischof, J., and Darby, D.A.: Mid- to Late Pleistocene ice drift in the western Arctic  
658 Ocean: Evidence for a different circulation in the Past, *Science*, 277, 74–78, 1997.
- 659 Carmack, E., Barber, D., Christensen, J., Macdonald, R., Rudels, B., and Sakshaug, E.:  
660 2006. Climate variability and physical forcing of the food webs and the carbon  
661 budget on pan-Arctic shelves, *Progress in Oceanography*, 71, 145–181, 2006.
- 662 Coachman, L.K., and Aagaard, K.: On the water exchange through Bering Strait,  
663 *Limnology and Oceanography*, 11, 44–59, 1966.
- 664 Danielson, S.L., Weingartner, T.J., Hedstrom, K.S., Aargaard, K., Woodgate, R.,  
665 Curchister, E., and Stabeno, P.J.: Coupled wind-forced controls of the  
666 Bering-Chukchi shelf circulation and the Bering Strait throughflow: Ekman  
667 transport, continental shelf waves, and variations of the Pacific-Arctic sea surface  
668 height gradient, *Progress in Oceanography*, 125, 40–61, 2014.



- 669 Darby, D.A., Ortiz, J.D., Polyak, L., Lund, S., Jakobsson, M., and Woodgate, R.A.: The  
670 role of currents and sea ice in both slowly deposited central Arctic and rapidly  
671 deposited Chukchi-Alaskan margin sediments, *Global and Planetary Change*, 68,  
672 58–72, 2009.
- 673 Darby, D.A., Myers, W.B., Jakobsson, M., and Rigor, I.: Modern dirty sea ice  
674 characteristic and sources: The role of anchor ice, *Journal of Geophysical Research*,  
675 116, C09008, 2011.
- 676 Darby, D.A., Ortiz, J.D., Grosch, C.E., and Lund, S.P.: 1,500-year cycle in the Arctic  
677 Oscillation identified in Holocene Arctic sea-ice drift, *Nature Geoscience*, 5, 897–  
678 900, 2012.
- 679 De Boer, A.M. and Nof, D.: The exhaust valve of the North Atlantic, *Journal of Climate*,  
680 17, 417–422, 2004.
- 681 de Vernal, A., Hillaire-Marcel, C., and Darby, D.A.: Variability of sea ice cover in the  
682 Chukchi Sea (western Arctic Ocean) during the Holocene, *Paleoceanography*, 20,  
683 PA4018, doi:10.1029/2005PA001157, 2005.
- 684 de Vernal A, Hillaire-Marcel C, Solignac S, et al.: Reconstructing sea ice conditions in  
685 the Arctic and sub-Arctic prior to human observations, *Geophysical Monograph*  
686 180, American Geophysical Union, Washington, p. 27–45, 2008.
- 687 de Vernal, A. et al.: Dinocyst-based reconstructions of sea ice cover concentration  
688 during the Holocene in the Arctic Ocean, the northern North Atlantic Ocean and its  
689 adjacent seas, *Quaternary Science Reviews*, 79, 111–121, 2013.
- 690 Dyke, A.S. and Savelle, J.M.: Holocene history of the Bering Sea bowhead whale  
691 (*Balaena mysticetus*) in Its Beaufort Sea summer grounds off southwestern Victoria  
692 Island, western Canadian Arctic, *Quaternary Research*, 55, 371–379, 2001.



- 693 Elias, S., Short, S.K., and Phillips, R.L.: Paleoecology of late-glacial peats from the  
694 Bering land bridge, Chukchi Sea shelf region, northwestern Alaska, Quaternary  
695 Research, 38, 371–378, 1992.
- 696 Elvelhøi, A. and Rønningsland, T.M.: Semiquantitative calculation of the relative  
697 amounts of kaolinite and chlorite by X-ray diffraction, Marine Geology, 27,  
698 M19-M23, 1978.
- 699 Farmer, J.R., Cronin, T.M., de Vernal, A., Dwyer, G.S., Keigwin, L.D., and Thunell,  
700 R.C.: Western Arctic Ocean temperature variability during the last 8000 years,  
701 Geophysical Research Letters, 38, L24602, 2011.
- 702 Frey, K.E., Perovich, D.K., and Light, B.: The spatial distribution of solar radiation  
703 under a melting Arctic sea ice cover, Geophysical Research Letters, 38, L22501,  
704 2011.
- 705 Funder, S. et al.: A 10,000-year record of Arctic Ocean sea-ice variability–View from  
706 the beach, Science, 333, 747–750, 2011.
- 707 Giles, K.A. et al.: Western Arctic Ocean freshwater storage increased by wind-driven  
708 spin-up of the Beaufort Gyre, Nature Geoscience, 5, 194–197, 2012.
- 709 Godfrey, J.S.: A sverdrup model of the depth-integrated flow for the ocean allowing for  
710 island circulations, Geophysical and Astrophysical Fluid Dynamics, 45, 89–112,  
711 1989.
- 712 Griffin, G.M. and Goldberg, E.D.: Clay mineral distributions in the Pacific Ocean. In  
713 Hill, M.N. (ed) The sea, III, p. 728-741, New York, Interscience Pub., 1963.
- 714 Gudkovitch, Z.M.: On the nature of the Pacific current in Bering Strait and the cause of  
715 its seasonal variations, Deep-Sea Research, 9, 507–510, 1962.



- 716 Harada, N.: Review: Potential catastrophic reduction of sea ice in the western Arctic  
717 Ocean: its impact on biogeochemical cycles and marine ecosystems, *Global and*  
718 *Planetary Change*, 136, 1–17, 2016.
- 719 Kaufman, D.S. et al.: Holocene climate changes in eastern Beringia (NW North  
720 America) – a systematic review of multi-proxy evidence, *Quaternary Science*  
721 *Reviews*, 147, 312–339, 2016.
- 722 Kalinenko, V.V.: Clay minerals in sediments of the Arctic Seas. *Lith. Min. Res.* 36,  
723 362–372. Translated from *Litologiya I Poleznye Iskopaemye* 4, 418–429, 2001.
- 724 Katsuki, K., Khim, B.-K., Itaki, T., Harada, N., Sakai, H., Ikeda, T., Takahashi, K.,  
725 Okazaki, Y., and Asahi, H.: Land–sea linkage of Holocene paleoclimate on the  
726 Southern Bering Continental Shelf, *The Holocene*, 19, 747–756, 2009.
- 727 Keigwin, L.D., Donnelly, J.P., Cook, M.S., Driscoll, N.W., and Brigham-Grette, J.:  
728 Rapid sea-level rise and Holocene climate in the Chukchi Sea, *Geology*, 34, 861–  
729 864, 2006.
- 730 Kobayashi, D., Yamamoto, M., Irino, T., Nam, S.-I., Park, Y.-H., Harada, N.,  
731 Nagashima, K., Chikita, K., and Saitoh, S.-I.: Distribution of detrital minerals and  
732 sediment color in western Arctic Ocean and northern Bering Sea sediments:  
733 Changes in the provenance of western Arctic Ocean sediments since the last glacial  
734 period, *Polar Science*, 10, 519–531, 2016.
- 735 Leduc, G., Vidal, L., Tachikawa, K., Rostek, F., Sonzogni, C., Beaufort, L. and Bard,  
736 E.: Moisture transport across Central America as a positive feedback on abrupt  
737 climatic changes, *Nature*, 445, 908–911, doi:10.1038/nature05578, 2007.
- 738 Lee, S.H., and Whitledge, T.E.: Primary and new production in the deep Canada Basin  
739 during summer 2002, *Polar Biology*, 28, 190–197, 2005.



- 740 Lisé-Pronovost, A., St-Onge, G., Brachfeld, S., Barletta, F., and Darby, D.:  
741 Paleomagnetic constraints on the Holocene stratigraphy of the Arctic Alaskan margin,  
742 *Global and Planetary Change*, 68, 85–99, 2009.
- 743 McKay, J. L. et al.: Holocene fluctuations in Arctic sea-ice cover: dinocyst-based  
744 reconstructions for the eastern Chukchi Sea, *Canadian Journal of Earth Sciences*, 45,  
745 1377–1397, 2008.
- 746 McNeely, R., Dyke, A.S., and Southon, J.R.: Canadian marine reservoir ages,  
747 preliminary data assessment, Open File Report–Geological Survey of Canada, 5049,  
748 no. 3, 2006.
- 749 Miller, G.H., Alley, R.B., Brigham-Grette, J., Fitzpatrick, J.J., Polyak, L., Serreze, M.C.,  
750 White, J.W.C.: Arctic amplification: can the past constrain the future? *Quaternary*  
751 *Science Reviews*, 29, 1779–1790, 2010.
- 752 Müller, G.: *Methods in Sedimentary Petrology*, Schweizerbart Science Publishers, 283p,  
753 Stuttgart, 1967.
- 754 Naidu, A.S., Creager, J.S., and Mowatt, T.C.: Clay mineral dispersal patterns in the  
755 North Bering and Chukchi Seas, *Marine Geology*, 47, 1-15, 1982.
- 756 Naidu, A.S. and Mowatt, T.C.: Sources and dispersal patterns of clay minerals in  
757 surface sediments from the continental shelf areas off Alaska, *Geological Society*  
758 *of America Bulletin*, 94, 841–854, 1983.
- 759 Nishino, S., Shimada, K., Itoh, M., and Chiba, S.: Vertical double silicate maxima in the  
760 sea-ice reduction region of the western Arctic Ocean: implications for an enhanced  
761 biological pump due to sea-ice reduction, *Journal of Oceanography*, 60, 871–883,  
762 2009.





- 763 Nishihara, M., Morri, H., and Koga, Y.: Structure determination of a quartet of novel  
764 tetraether lipids from *Methanobacterium thermoautotrophicum*, *Journal of*  
765 *Biochemistry*, 101, 1007–1015, 1987.
- 766 Nwaodua, E., Ortiz, J.D., and Griffith, E.M.: Diffuse spectral reflectance of surficial  
767 sediments indicates sedimentary environments on the shelves of the Bering Sea and  
768 western Arctic, *Marine Geology*, 355, 218–233, 2014.
- 769 Olsen, J., Anderson, N.J., and Knudsen, M.F.: Variability of the North Atlantic  
770 Oscillation over the past 5,200 years, *Nature Geoscience*, 5, 808–812, 2012.
- 771 Ortiz, J.D., Polyak, L., Grebmeier, J.M., Darby, D., Eberl, D.D., Naidu, S., and Nof, D.:  
772 Provenance of Holocene sediment on the Chukchi-Alaskan margin based on  
773 combined diffuse spectral reflectance and quantitative X-Ray Diffraction analysis,  
774 *Global Planetary Change*, 68, 73–84, 2009.
- 775 Ortiz, J.D., Nof, D., Polyak, L., St-Onge, G., Lisé-Pronovost, A., Naidu, S., Darby, D.,  
776 and Brachfeld, S.: The late Quaternary flow through the Bering Strait has been  
777 forced by the Southern Ocean winds, *Journal of Physical Oceanography*, 42, 2014–  
778 2029, 2012.
- 779 Osterberg, E.C., Mayewski, P.A., Fisher, D.A., Kreutz, K.J., Maasch, K.A., Sneed, S.B.,  
780 and Kelsey, E.: Mount Logan ice core record of tropical and solar influences on  
781 Aleutian Low variability: 500–1998 A.D. *Journal of Geophysical Research*,  
782 *Atmosphere*, 119, 11,189–11,204, doi:10.1002/2014JD021847, 2014.
- 783 Overland, J.O., Adams, J. M., and Bond, N.: Decadal variability of the Aleutian Low  
784 and its relation to high-latitude circulation, *Journal of Climate*, 12, 1542–1548,  
785 1999.



- 786 Paillard, D., Labeyrie, L., and Yion, P.: Macintosh program performs time-series  
787 analysis, EOS Trans. AGU 77, 379, 1996.
- 788 Park, Y.-H., Yamamoto, M., Polyak, L., and Nam, S.-I.: Glycerol dialkyl glycerol  
789 tetraether variations in the northern Chukchi Sea, Arctic Ocean, during the  
790 Holocene, Biogeosciences Discussion, doi:10.5194/bg-2016-529, 2016.
- 791 Petschick, R.: MacDiff 4.2.6. [online] available at  
792 <http://www.geol-pal.uni-frankfurt.de/Staff/Homepages/Petschick/MacDiff/MacDiff>  
793 %20Latest%20infoE.html, 2000.
- 794 Phillips, R.P., and Grantz, A.: Regional variations in provenance and abundance of  
795 ice-rafted clasts in Arctic Ocean sediments: implications for the configuration of  
796 late Quaternary oceanic and atmospheric circulation in the Arctic, Marine Geology  
797 172, 91–115, 2001.
- 798 Pickart, R.S.: Shelfbreak circulation in the Alaskan Beaufort Sea: Mean structure and  
799 variability, Journal of Geophysical Research 109, C04024, 2004.
- 800 Pickart, R.S., Pratt, L.J., Torres, D.J., Whitledge, T.E., Proshutinsky, A.Y., Aagaard, K.,  
801 Agnewd, T.A., Moore, G.W.K., and Dail, H.J.: Evolution and dynamics of the flow  
802 through Herald Canyon in the western Chukchi Sea, Deep-Sea Research II, 57, 5–  
803 26, 2010.
- 804 Polyak, L., Bischof, J., Ortiz, J.D., Darby, D.A., Channell, J.E.T., Xuan, C., Kaufman,  
805 D.S., Løvile, R., Schneider, D., Eberl, D.D., Adler, R.E., and Council, E.A.: Late  
806 Quaternary stratigraphy and sedimentation patterns in the western Arctic Ocean,  
807 Global and Planetary Change, 68, 5–17, 2009.



- 808 Polyak, L., Belt, S., Cabedo-Sanz, P., Yamamoto, M., and Park, Y.-H.: Holocene  
809 sea-ice conditions and circulation at the Chukchi-Alaskan margin, Arctic Ocean,  
810 inferred from biomarker proxies, *The Holocene*, 26, 1810–1821, 2016.
- 811 Porter, S.E.: Assessing whether climate variability in the Pacific Basin influences the  
812 climate over the North Atlantic and Greenland and modulates sea ice extent, Ph.D.  
813 Thesis, Ohio State University, 222 p, 2013.
- 814 Proshutinsky, A.Y. and Johnson, M.A.: Two circulation regimes of the wind-driven  
815 Arctic Ocean, *Journal of Geophysical Research*, 102 (C6), 12493–12514, 1997.
- 816 Qin, W., Amin, S.A., Martens-Habbena, W., Walker, C.B., Urakawa, H., Devol, A.H.,  
817 Ingalls, A.E., Moffett, J.M., Armbrust, E.V., and Stahl, D.A.: Marine  
818 ammonia-oxidizing archaeal isolates display obligate mixotrophy and wide ecotypic  
819 variation. *Proceedings of the National Academy of Science*, 111, 12504–12509,  
820 2014.
- 821 Reimer, P.J., et al.: Intcal13 and Marine13 radiocarbon age calibration curves 0–50,000  
822 years cal BP., *Radiocarbon*, 55, 1869–1887, 2013.
- 823 Richter, I. and Xie, S.: Moisture transport from the Atlantic to the Pacific basin and its  
824 response to North Atlantic cooling and global warming, *Climate Dynamics*, 35,  
825 551–566, doi:10.1007/s00382-009-0708-3, 2010.
- 826 Rigor, I. G. et al.: Response of sea ice to the Arctic Oscillation, *Journal of Climate*, 15,  
827 2648–2663, 2002.
- 828 Rimbu, N., Lohmann, G., Kim, J.-H., Arz, H.W., and Schneider, R.: Arctic/North  
829 Atlantic Oscillation signature in Holocene sea surface temperature trends as  
830 obtained from alkenone data, *Geophysical Research Letters*, 30, 1280.  
831 doi:10.1029/2002GL016570, 2003.



- 832 Roach, A.T., Aagaard, K., Pease, C.H., Salo, S.A., Weingartner, T., Pavlov, V., and  
833 Kulakov, M.: Direct measurements of transport and water properties through  
834 Bering Strait, *Journal of Geophysical Research*, 100, 18433–18457, 1995.
- 835 Sakshaug, E.: Primary and secondary production in the Arctic ocean, In: Stein, R.,  
836 Macdonald, R.W. (Eds.), *The Organic Carbon Cycle in the Arctic Ocean*, Springer,  
837 Berlin, pp. 57–81, 2004.
- 838 Sandal, C. and Nof, D.: The Collapse of the Bering Strait Ice Dam and the Abrupt  
839 Temperature Rise in the Beginning of the Holocene, *Journal of Physical*  
840 *Oceanography*, 38, 1979–1991, 2008.
- 841 Sarnthein, M., Gebhardt, H., Kiefer, T., Kucera, M. Cook, M., and Erlenkeuser, H.:  
842 Mid Holocene origin of the sea-surface salinity low in the subarctic North Pacific,  
843 *Quaternary Science Reviews*, 23, 2089–2099, 2004.
- 844 Screen, J.A. and Simmonds, I.: The central role of diminishing sea ice in recent Arctic  
845 temperature amplification, *Nature*, 464, 1334–1337, 2010.
- 846 Shimada, K., Carmack, E., Hatakeyama, K., and Takizawa, T.: Varieties of shallow  
847 temperature maximum waters in the Western Canadian Basin of the Arctic Ocean,  
848 *Geophysical Research Letters*, 28, 3441–3444, 2001.
- 849 Shimada, K., Kamoshida, T., Itoh, M., Nishino, S., Carmack, E., McLaughlin, F.,  
850 Zimmermann, S., and Proshutinsky, A.: Pacific Ocean inflow: Influence on  
851 catastrophic reduction of sea ice cover in the Arctic Ocean, *Geophysical Research*  
852 *Letters*, 33, L08605, 2006.
- 853 Shtokman, V.B.: Vliyanie vetra na techeniya v Beringovo Prolive, prichiny ikh  
854 bol'shikh skorostei i preobladayueshego severnogo napravleniya, *Trans. Inst.*  
855 *Okeanolog.*, Akad. Nauk SSSR, 25, 171–197, 1957.



- 856 Singh, H.K.A., Donohoe, A., Bitz, C.M., Nusbaumer, J., and Noone, D.C.: Greater  
857 aerial moisture transport distances with warming amplify interbasin salinity  
858 contrasts. *Geophysical Research Letters* 43, 8677–8684,  
859 doi:10.1002/2016GL069796, 2016.
- 860 Stein R.: *Developments in Marine Geology: Arctic Ocean Sediments: Processes,*  
861 *Proxies, and Paleoenvironment*, Elsevier, Amsterdam, 529p, 2008.
- 862 Stein, R., Fahl, K., Schade, I., Nanerung, A., Wassmuth, S., Niessen, F., and Nam, S.-I.:  
863 Holocene variability in sea ice cover, primary production, and Pacific-Water inflow  
864 and climate change in the Chukchi and East Siberian Seas (Arctic Ocean), *Journal*  
865 *of Quaternary Science*, 32, 362–379, 2017.
- 866 Steinman, B.A., Abbott, M.B., Mann, M.E., Ortiz, J.D., Feng, S., Pompeani, D.P.,  
867 Stansell, N.D., Anderson, L., Finney, B.P., and Bird, B.W.: Ocean-atmosphere  
868 forcing of centennial hydroclimate variability in the Pacific Northwest,  
869 *Geophysical Research Letters*, 41, doi:10.1002/2014GL059499, 2014.
- 870 Steinhilber, F., Beer, J., and Fröhlich, C.: Total solar irradiance during the Holocene,  
871 *Geophysical Research Letters*, 36, L19704, doi:10.1029/2009GL040142, 2009.
- 872 Stigebrandt, A.: The North Pacific: A global-scale estuary, *Journal of Physical*  
873 *Oceanography*, 14, 464–470, 1984.
- 874 Vare L.L., Masse G., and Gregory, T.R.: Sea ice variations in the central Canadian  
875 Arctic Archipelago during the Holocene, *Quaternary Science Reviews*, 28, 1354–  
876 1366, 2009.
- 877 Viscosi-Shirley, C., Mammone, K., Pisia, N., and Dymond, J.: Clay mineralogy and  
878 multi-element chemistry of surface sediments on Siberian-Arctic shelf: implications



- 879 for sediment provenance and grain size sorting, *Continental Shelf Research*, 23,  
880 1175–1200, 2003.
- 881 Vogt, C.: Regional and temporal variations of mineral assemblages in Arctic Ocean  
882 sediments as climatic indicator during glacial/interglacial changes, *Reports on Polar*  
883 *Research*, 251, 1–309, 1997.
- 884 Volkman, J.K.: A review of sterol markers for marine and terrigenous organic matter,  
885 *Organic Geochemistry*, 9, 83–99, 1986.
- 886 Wahsner, M., Müller, C., Stein, R., Ivanov, G., Levitan, M., Shekekhova, E., and  
887 Tarasov, G.: Clay-mineral distribution in surface sediments of Eurasian Arctic  
888 Ocean and continental margin as indicator for source areas and transport pathways  
889 – a synthesis, *Boreas*, 28, 216–233, 1999.
- 890 Walsh, J.J., and Dieterle, D.A.: CO<sub>2</sub> cycling in the coastal ocean. I. A numerical  
891 analysis of the southeastern Bering Sea, with applications to the Chukchi sea and  
892 the northern Gulf of Mexico, *Progress in Oceanography*, 34, 335–392, 1994.
- 893 Watanabe, E., Onodera, J., Harada, N., Honda, M., Kimoto, K., Kikuchi, T., Nishino, S.,  
894 Matsuno, K., Yamaguchi, A., Ishida, A., and Kishi, J.M.: Enhanced role of eddies  
895 in the Arctic marine biological pump. *Nature Communications*,  
896 <http://dx.doi.org/10.1038/ncomms4950>, 2014.
- 897 Weingartner, T., Aagaard, K., Woodgate, R., Danielson, S., Sasaki, Y., and Cavalieri,  
898 D.: Circulation on the north central Chukchi Sea shelf, *Deep-Sea Research II*, 52,  
899 3150–3174, 2005.
- 900 Winsor, P. and Chapman, D.C.: Pathways of Pacific water across the Chukchi Sea: A  
901 numerical model study, *Journal of Geophysical Research*, 109, C03002,  
902 doi:10.1029/2003JC001962, 2004.



903 Yamamoto-Kawai, M., Carmack, E., and McLaughlin, F.: Nitrogen balance and Arctic  
904 throughflow, *Nature*, 443, 43, 2006



905 **Figure captions**

906

907 Fig. 1. Index map showing location of cores ARA02B 01A-GC (this study),  
908 HLY0501-05JPC/TC (this study and Farmer et al., 2011), HLY0501-06JPC (this study  
909 and Ortiz et al., 2009), and HLY0205-GGC19 (Farmer et al., 2011), as well as surface  
910 sediment samples (Kobayashi et al., 2016, with additions). BSI = Bering Strait inflow,  
911 BC = Barrow Canyon, HN = Hanna Shoal, and HR = Herald Shoal. BG = Beaufort  
912 Gyre, ACC = Alaskan Coastal Current, SBC = Subsurface Boundary Current, ESCC =  
913 East Siberian Coastal Current, TPD = Transpolar Drift. Red, yellow and blue arrows  
914 indicate BSI branches. AO+ and AO- indicate circulation in the positive and negative  
915 phases of the Arctic Oscillation, respectively.

916

917 Fig. 2. Spatial distributions of the diffraction intensity ratios of (A) feldspar to quartz  
918 (Q/F), and of (B) chlorite+kaolinite and (C) chlorite to illite (CK/I and C/I, respectively)  
919 of bulk sediments, and (D) the longitudinal distribution of the Q/F ratio in the western  
920 Arctic (>65°N) and (E) the latitudinal distribution of the CK/I and C/I ratios in the  
921 Bering Sea and the western Arctic (>150°W). The C/I ratio could not be determined in  
922 some coarse-grained sediment samples. Data from Kobayashi et al. (2016) with  
923 additions for the Beaufort Sea (See supplementary Table 1 in more detail).

924

925 Fig. 3. Depth profile in (A) quartz/feldspar (Q/F) ratio, (chlorite + kaolinite)/illite  
926 (CK/I), chlorite/illite (C/I) and kaolinite/illite (K/I) ratios with 1σ-intervals (analytical  
927 error) in cores (A) ARA02B 01A-GC, (B) HLY0501-05JPC/TC and (C)





928 HLY0501-06JPC (Supplementary Tables 2–4). “D” indicates a dolomite-rich layer.

929 Note that the depth scale of 01A-GC is doubled.

930

931 Fig. 4. Changes in (A) quartz/feldspar (Q/F) ratio and the June insolation at 75°N, (B)

932 (chlorite + kaolinite)/illite (CK/I) and chlorite/illite (C/I) ratios and (C) linear

933 sedimentation rates (LSR) in cores ARA02B 01A-GC, HLY0501-05JPC/TC and

934 HLY0501-06JPC during the last ca. 9.3 ka.

935

936 Fig. 5. Conceptual map showing the distribution of summer sea ice and the rotation of

937 the Beaufort Gyre (BG) in the early, middle and late Holocene, inferred from the

938 quartz/feldspar (Q/F) proxy record. Also shown is the Bering Strait inflow (BSI)

939 intensity inferred from the (chlorite + kaolinite)/illite (CK/I) and chlorite/illite (C/I)

940 ratios. Red arrow indicates the drift path of Kara Sea grains (KSG; Darby et al., 2012).

941

942 Fig. 6. Max Entropy power spectra of variation in the quartz/feldspar (Q/F) and

943 chlorite/illite (C/I) ratios in core ARA02B 01A-GC (N=85, m=21) and

944 HYL0501-06JPC (N=79, m=22) during 1.4–7.9 ka and the total solar irradiance (N=932,

945 m=140)(Steinhilber et al., 2009) during the last 9.3 ka.

946

947 Fig. 7. Detrended variations in the solar irradiance (TSI; Steinhilber et al., 2009), the

948 quartz/feldspar (Q/F) ratio in logarithmic scale in cores ARA02B 01A-GC and

949 HYL0501-06JPC and the chlorite/illite (C/I) ratio in core ARA02B 01A-GC during the

950 Holocene, with 400-year moving averages and 1,000-year filtered variations indicated

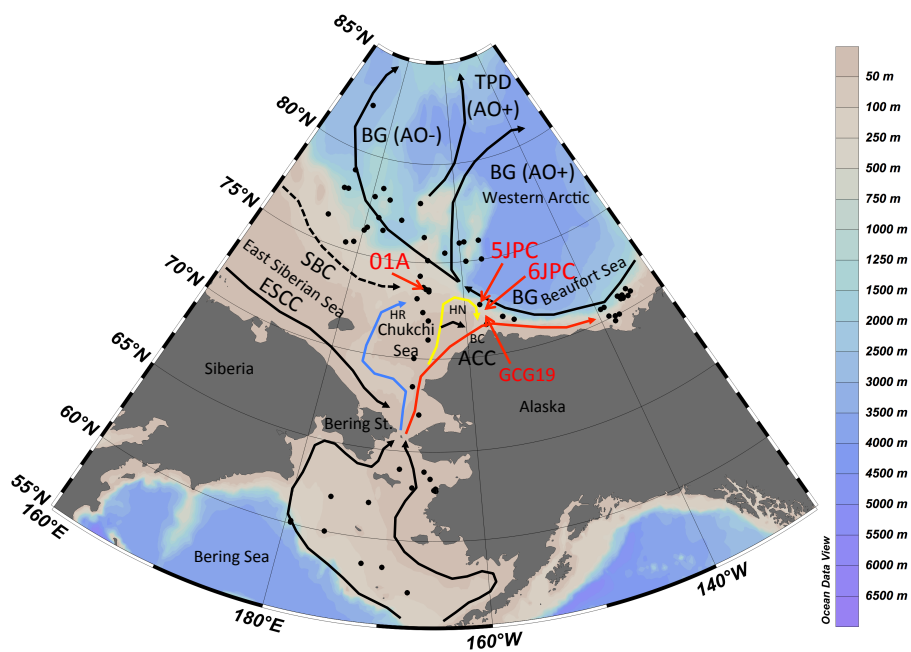


951 by dark colored and black lines, respectively. The detrended values were obtained by  
952 cubic polynomial regression.

953

954 Fig. 8. Changes in (A) (chlorite + kaolinite)/illite (CK/I) and chlorite/illite (C/I) ratios,  
955 PIP<sub>25</sub> (P<sub>D</sub>IP<sub>25</sub> and P<sub>B</sub>IP<sub>25</sub> based on IP<sub>25</sub> and dinosterol or brassicasterol concentrations)  
956 indices (Stein et al., 2017), and isoprenoid GDGT (Park et al., 2016) and brassicasterol  
957 concentrations (Stein et al., 2017) in core ARA02B 01A-GC, (B) CK/I and C/I ratios in  
958 core HLY0510-5JPC/TC, IP<sub>25</sub> concentrations in core HLY0510-5JPC (Polyak et al.,  
959 2016), mean annual sea ice cover concentration (scale from 0 to 10) estimated from  
960 dinoflagellate cyst assemblages in cores 05JPC and GGC19 (Farmer et al., 2011; de  
961 Vernal et al., 2013).

962

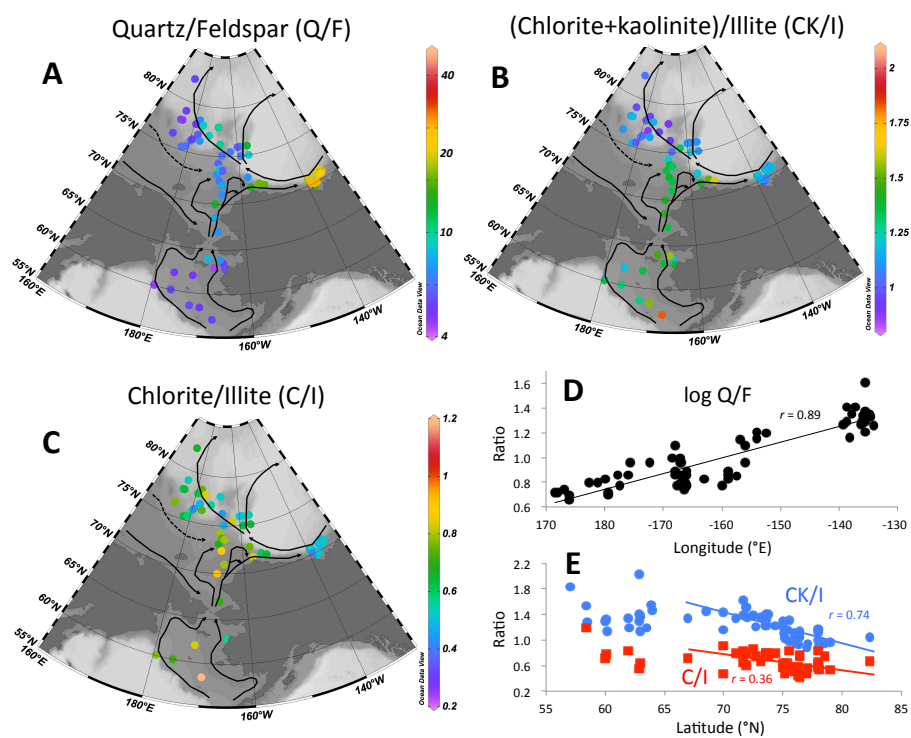


963

964

965 Fig. 1

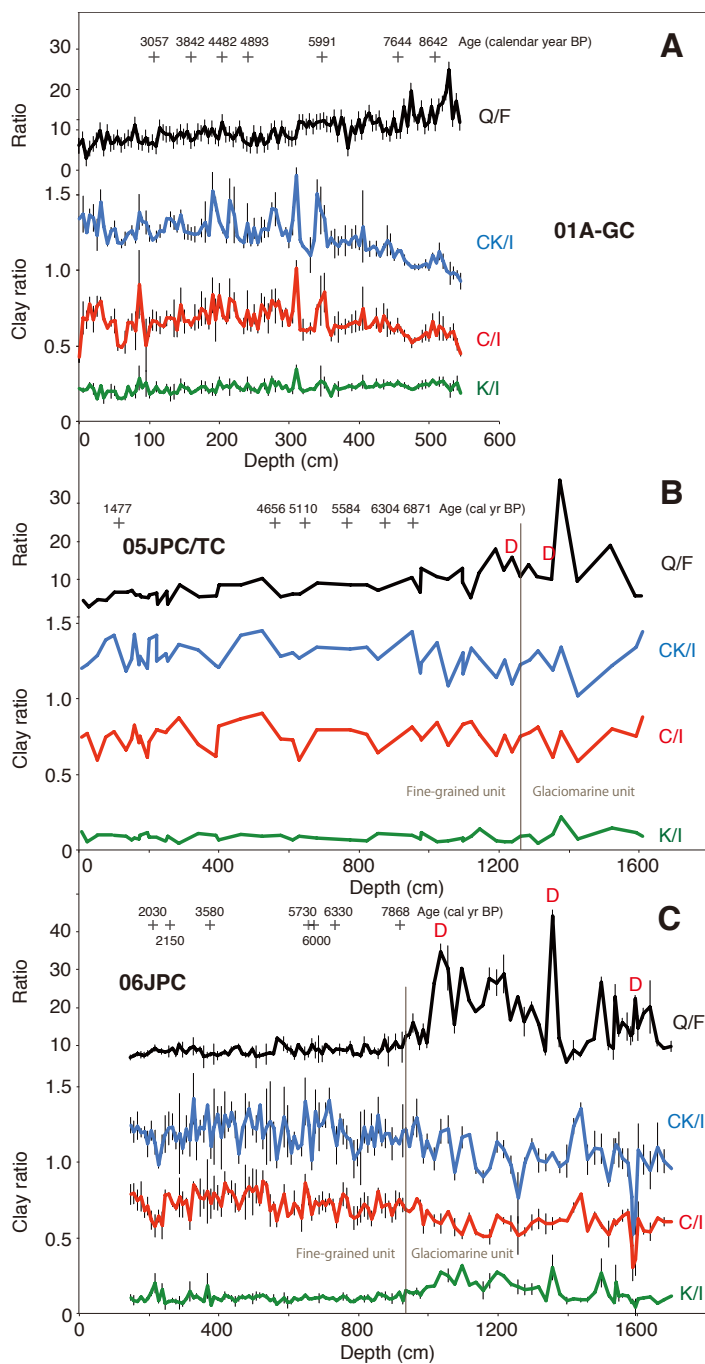
966



967

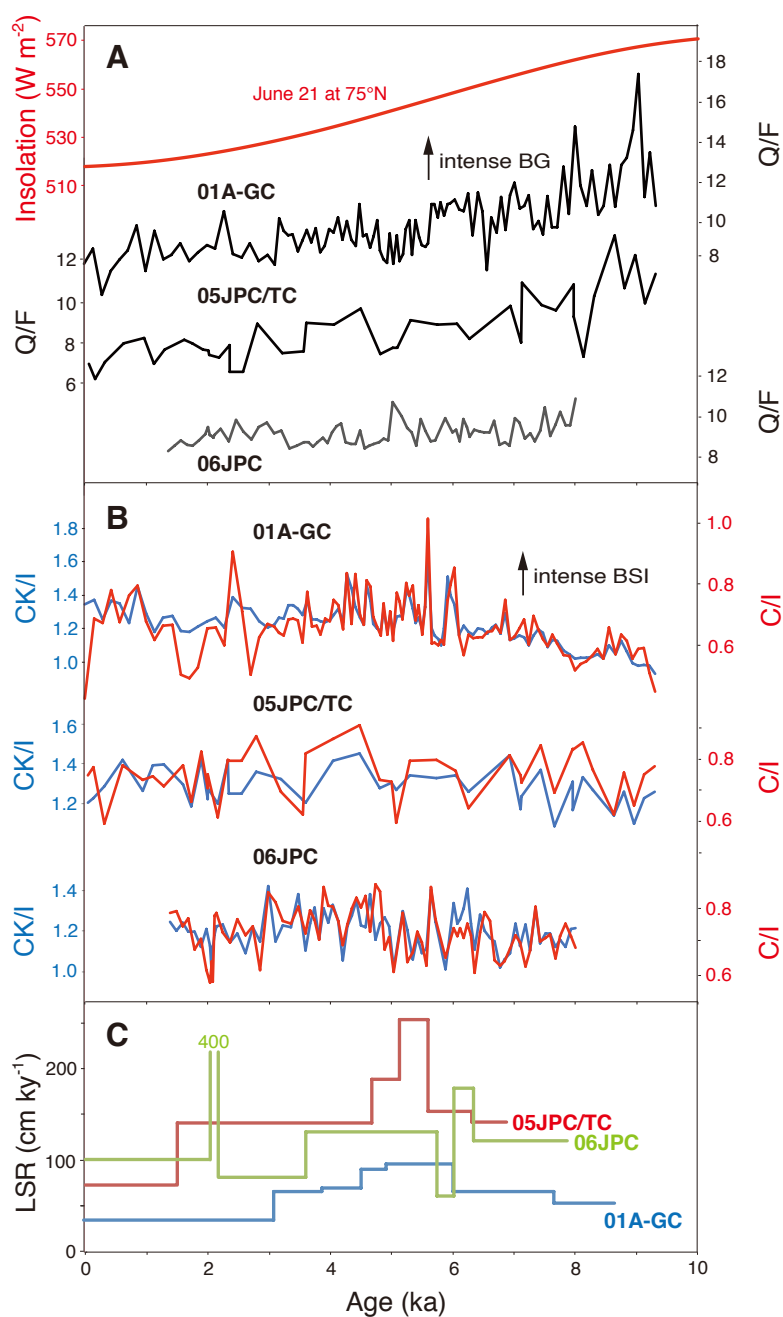
968 Fig. 2

969



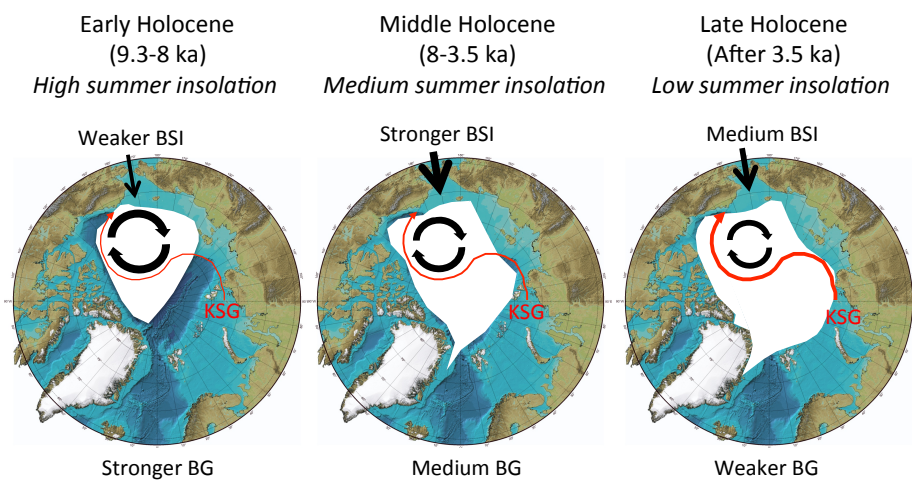
970

971 Fig. 3



972

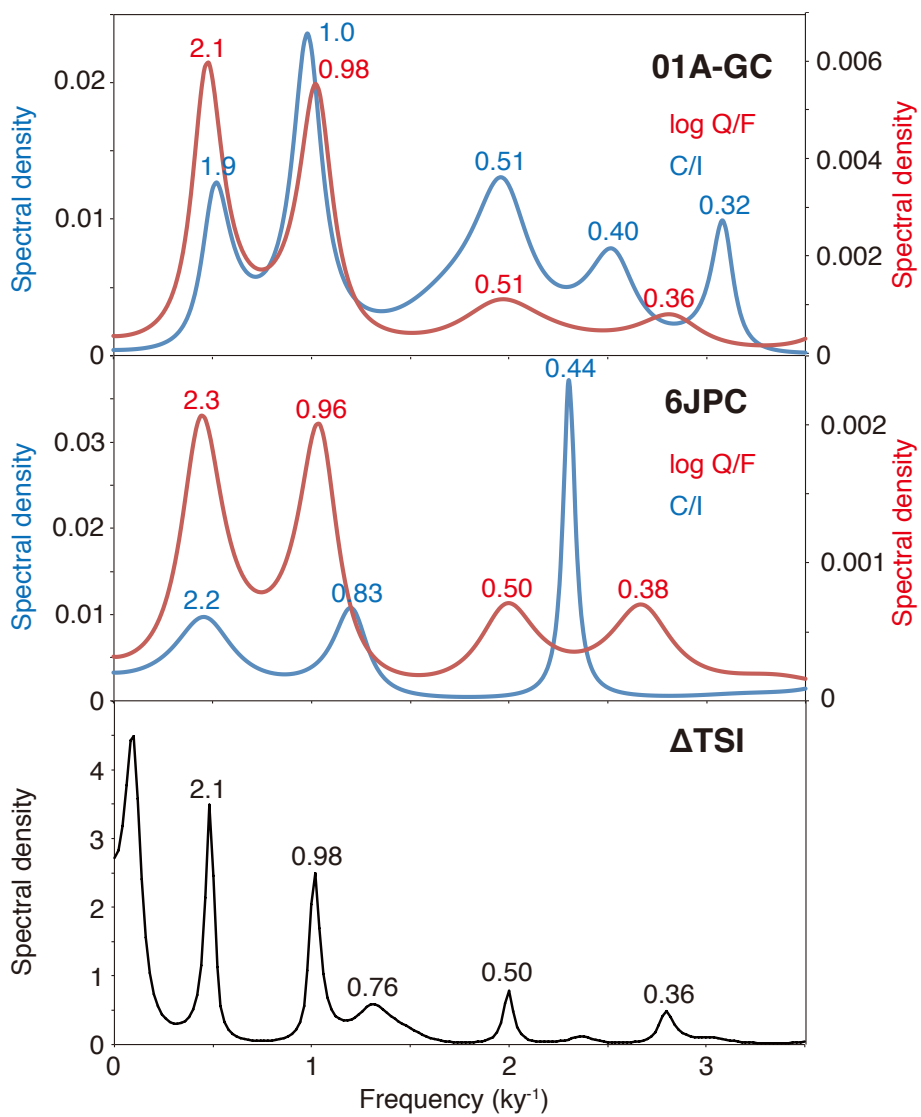
973 Fig. 4.



974

975 Fig. 5

976

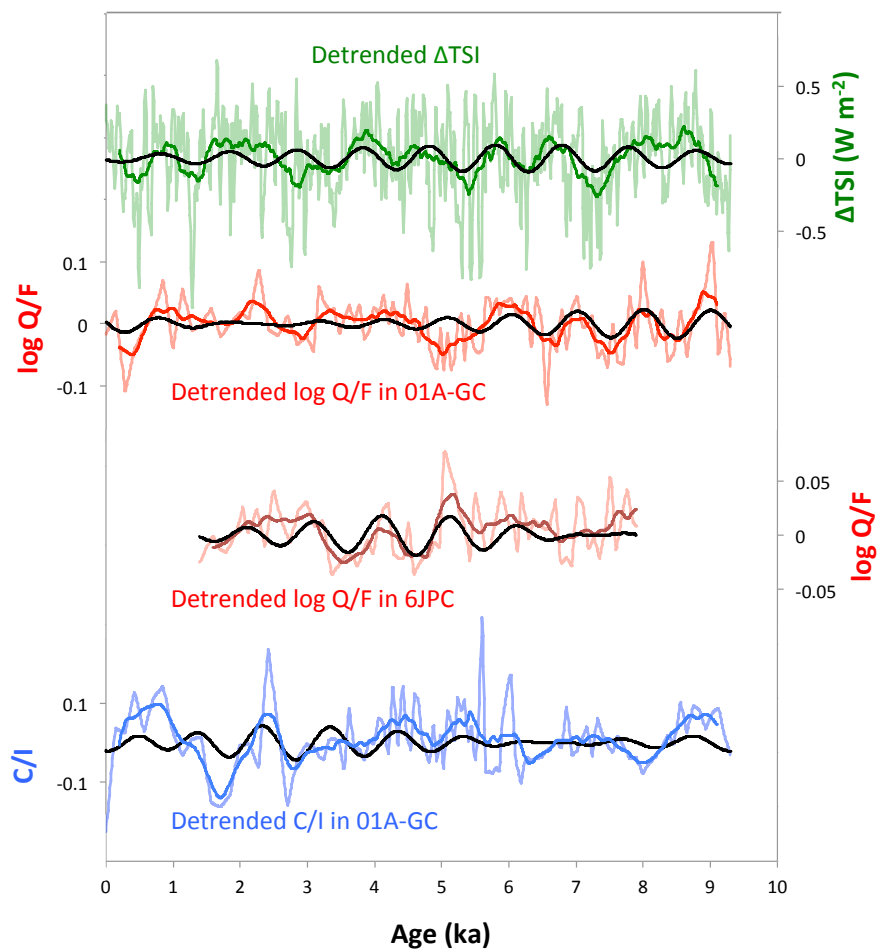


977

978 Fig. 6

979

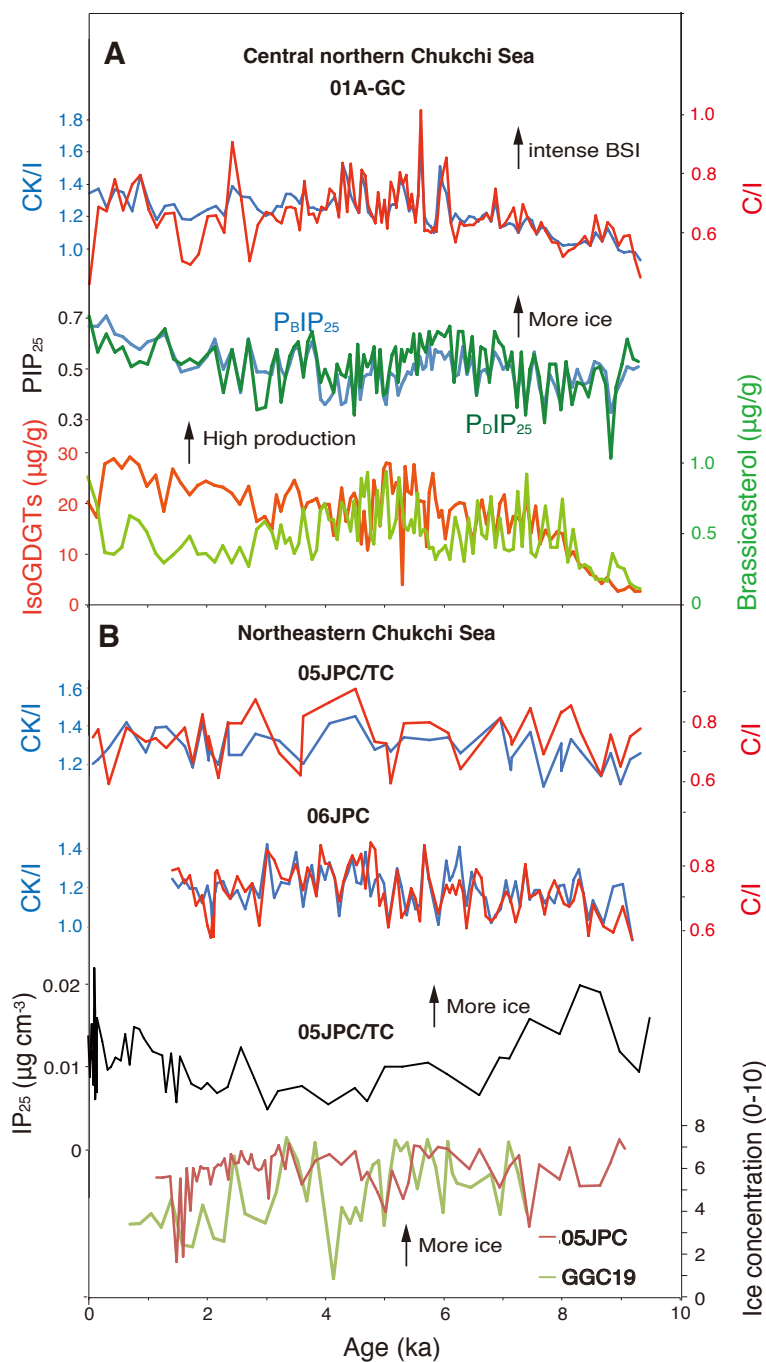




980

981 Fig. 7

982



983

984 Fig. 8